Canonical Variational Transition-State Theory Study of the CF 3 CH 2 CH 3 + OH Reaction †

ARTICLE *in* THE JOURNAL OF PHYSICAL CHEMISTRY B · FEBRUARY 2008

Impact Factor: 3.3 · DOI: 10.1021/jp075298v · Source: PubMed

Canonical Variational Transition-State Theory Study of the $CF_3CH_2CH_3$ + OH Reaction†

Àngels González-Lafont* and José M. Lluch

Departament de Química, Universitat Autònoma de Barcelona, 08193 Bellaterra, Barcelona, Spain.

Adrián Varela-Álvarez and José A. Sordo

Laboratorio de Química Computacional, Departamento de Química Física y Analítica, Universidad de Oviedo, 33006 Oviedo, Principado de Asturias, Spain.

Received: July 7, 2007; In Final Form: October 11, 2007

Variational transition-state theory rate constants with multidimensional tunneling contributions using the small curvature method have been calculated for the $CF_3CH_2CH_3$ (HFC-263fb) + OH reaction over a temperature range from 200 to 373 K. The mPW1B95-41.0 hybrid functional, parametrized by Albu and Swaminathan to generate theoretical rate constants nearly identical to the experimental values for the CH_3F + OH reaction, has been used in conjunction with the 6-31+G** basis set to explore the potential energy surface of the title reaction. The good agreement found between theoretical predictions and the experimental data available suggests that the present approach is an excellent option to obtain high-quality results at low computational cost for direct dynamics studies of hydrogen abstraction reactions from complex hydrofluorocarbons. The reliability of the structure activity relationship used to estimate rate constant values for OH reactions with hydrofluorocarbons is also discussed in detail.

Introduction

Chlorofluorocarbons (CFCs) are recognized as the major source of chlorine in the stratosphere, which is a main cause of ozone depletion.[1] Furthermore, CFCs are well-known greenhouse gases. Therefore, since CFCs have industrial and housewares applications, a more environmentally friendly family of compounds is needed to substitute CFCs. Among others, hydrofluorocarbons (HFCs) have been used as alternatives to CFCs because the absence of chlorine (and bromine) from their composition make them ozone-friendly. On the other hand, HFCs still contain C−F bonds that could contribute to global warming, but, unlike CFCs, they are not inert gases, since they contain C−H bonds. Indeed, HFCs are susceptible to suffer attack in the troposphere, mainly due to degradation by hydroxyl radicals.[2] Consequently, HFCs have shorter lifetimes than CFCs, i.e., their contribution to global warming is expected to be less important.

For any HFC, the starting reaction in the degradation mechanism is a hydrogen abstraction process by OH. In particular, for $CF_3CH_2CH_3$ (HFC-263fb), we have the following two H-abstraction reactions:

$$CF_3CH_2CH_3 + OH \rightarrow CF_3CHCH_3 + H_2O \qquad (R1)$$

$$CF_3CH_2CH_3 + OH \rightarrow CF_3CH_2CH_2 + H_2O \qquad (R2)$$

Thus, it is desirable to estimate how fast these reactions proceed if the OH-driven lifetime for HFC-263fb is needed to infer whether this HFC compound is a more environmentally friendly substitute of CFCs, as suggested.

In order to validate the suitability of the different HFCs as alternatives to CFCs, several experimental studies have been carried out.[3−7] Three experimental techniques have been mostly used: discharge flow, laser flash photolysis, and relative rate measurements. None of them can be considered as a routine or a low-cost technique and, consequently, for many compounds, the rate constants have not yet been experimentally measured. For this reason, some authors,[8] mainly Atkinson and co-workers,[9] tried to use the information on the reaction rates of several model reactions in order to obtain empirical equations that could predict the rate constants for OH reactions with specific species of particular interest. However, the original general structure activity relationship (SAR) method developed by Atkinson and co-workers[9] did not yield good results for HFCs and halogenated ethers. The cause of disagreement has been attributed to the limited set of reference compounds and to the fact that the SAR method only considers next-neighbor atomic groups. Consequently, a number of modifications have been proposed,[4,5,10] and other empirical estimation methods have been developed.[11] In addition, several authors have developed correlations between the kinetic parameters of those OH radical reactions and the molecular parameters of HFCs.[12,13]

From a theoretical point of view, several HFCs have been studied, mainly fluoromethanes and fluoroethanes[14−25] and, very recently, fluoropropanes.[26] These studies can be classified as those based on the conventional transition-state theory (TST) and, on the other hand, the studies based on the generalized transition state theory.

In particular, for the OH radical attack on $CF_3CH_2CH_3$ studied in this paper, two experimental studies have been reported:

(i) Nelson and co-workers[6] used discharge flow technique with laser-induced fluorescence detection (DF-LIF) of OH radicals in order to obtain a rate constant at 298 K. The value of the rate constant reported by Nelson and co-workers is $k_{exp}^{Nel}(298\ K) = 4.20 \times 10^{-14}\ cm^3\ molecule^{-1}\ s^{-1}$.

(ii) Ravishankara and co-workers[7] used pulsed laser photolysis with laser-induced fluorescence detection (PLP-LIF) of the OH

† Part of the "James T. (Casey) Hynes Festschrift".

* Corresponding author. E-mail: angels@klingon.uab.es.

10.1021/jp075298v CCC: $40.75
Published on Web 12/15/2007

radicals. The measurements were carried out between 238 and 373 K, and an unweighted linear least-squares fit of the corresponding Arrhenius plot yielded

$$k_{exp}^{Rav}(T) = (4.36 \pm 0.63) \times 10^{-12} \exp[(-1293 \pm 42)/T] \text{ cm}^3 \text{ molecule}^{-1} \text{ s}^{-1}$$

Then, k_{exp}^{Rav} (298 K) = 5.55×10^{-14} cm^3 molecule^{-1} s^{-1}, which is a slightly higher value than the one measured by Nelson and co-workers.[6] In addition, Ravishankara and co-workers used the SAR method to evaluate the contribution of each site of the molecule toward the global rate coefficient. In accordance with those calculations using the SAR method derived by Tokuhashi et al.,[10] the contribution of the CH_2 group is only 7%, while the rest of the reaction is due to the CH_3 group. In contrast, the SAR calculations reported by Ravishankara and co-workers using DeMore's[4] group contributions indicate that both CH_2 and CH_3 groups contribute almost equally to the overall reaction. In view of this discrepancy, Ravishankara and co-workers indicate that the conclusion of DeMore's method appears to be more reasonable.

As far as we know, no theoretical calculations of the rate constants for the OH radical attack on $CF_3CH_2CH_3$ have been reported. The aim of the present work is to calculate the global rate constants for this reaction using variational transition-state theory with multidimensional tunneling contributions. In addition, the branching ratio between the two H-abstraction reactions, a magnitude that has not been obtained from experiments, will be given. The comparison of our theoretical result with the two contradictory SAR values will help to solve the controversy on CH_2 versus CH_3 group contributions to the global rate constant of the title reaction.

Method Of Calculation

Electronic Structure Calculations. All electronic structure calculations were carried out using the Gaussian 03 suite of programs.[27]

The nature of the located stationary points was characterized according to the number of imaginary vibrational frequencies (0 for a minimum or 1 for a saddle point). Molecular geometry optimizations and harmonic vibrational frequencies were calculated using the mPW1B95-41.0[25a,28,29] hybrid meta-GGA[30] functional in conjunction with the 6-31+G(d,p) basis set. This functional combines a modified Perdew−Wang exchange functional with 41.0% of Hartree−Fock (HF) exchange, and uses meta-GGA Becke95 for the correlation counterpart.

The percentage of HF exchange was adjusted by Albu and Swaminathan[25a] following the specific-reaction-parameter (SRP) approach[31] in order to provide calculated rate constants within an acceptable range (10%) of the experimental rate constant at 340 K for the model reaction:

$$CFH_3 + OH \rightarrow CFH_2 + H_2O$$

The analysis of the accuracy of that new hybrid functional method was carried out using a set of experimental rate constants over a wide temperature range. In the same paper,[25a] two other hybrid functionals were developed in the same way: mPW1PW91-35.7[25a,28,32] (35.7% of HF exchange) and B1B95-37.0[25a,29,33,34] (37.0% of HF exchange). It is useful to compare these three new functionals with the corresponding ones previously developed by Truhlar and co-workers (K methods): MPWB1K (mPW1B95-44.0 with the notation by Albu and Swaminathan), MPW1K (mPW1PW91-42.8), and BB1K (B1B95-42.0).[35−37] The smallest difference between the Truhlar and co-workers' and Albu−Swaminathan parametrizations, i.e., the smallest change on the percentage of HF exchange (X), occurs for the mPW1B95-X functional. For this reason and remembering that Truhlar and co-workers developed their functionals for general purposes (thermochemistry, thermochemical kinetics, and noncovalent interactions), the mPW1B95-41.0 functional seems to be the most suitable.

While the present work was in progress, a new SRP study was reported by Albu and Swaminathan.[25b] In that paper, the authors optimized the HF exchange percentage to obtain three new functionals (mPW1PW91-33.5, mPW1B95-38.5, and B1B95-34.8) for the model reaction

$$CF_3H + OH \rightarrow CF_3 + H_2O$$

The small differences found between the two SRP sets developed by Albu and Swaminathan[25] support the hypothesis of transferability,[24] which is the basis of the present work.

Atomic Net Charges. Atomic net charges have been calculated by means of the integration of the electronic charge density over the corresponding atomic basins as done by the PROAIM algorithm in the framework of the quantum theory of atoms in molecules (QTAIM).[38] The calculations were carried out with the AIMPAC suite of programs.[39]

Dynamical Calculations. The dynamical calculations were carried out using variational transition-state theory with multidimensional tunneling (VTST/MT)[40] contributions. In the canonical variational transition-state theory (CVT), the rate constant,[40,41] $k^{CVT}(T)$, is obtained by minimizing the generalized rate constant $k^{GT}(T,s)$ (at temperature T) along the reaction path:

$$k^{CVT}(T) = k^{GT}(T,s_*) = \min_s\{k^{GT}(T,s)\} \quad (1)$$

where s denotes the distance along the minimum energy path (MEP)[41,42] in an isoinertial mass-scaled coordinate system with a scaling mass equal to 1 amu, and s_* is the value of s that minimizes the generalized rate constant (or that maximizes the generalized activation free energy) along the reaction path (MEP) at temperature T. The CVT rate constant is given[40,41] by

$$k^{CVT}(T) = \sigma \frac{k_B T Q^{GT}(T,s_*)}{h \quad Q^R(T)} \exp(-V(s_*)/k_B T) \quad (2)$$

where σ is the symmetry number, k_B is the Boltzmann's constant, h is the Planck's constant, $V(s_*)$ is the classical potential energy at s_* with zero energy at the overall classical energy of reactants (that is, without the zero point energy contributions that will be included in the partition functions), $Q^R(T)$ is the reactant partition function per unit volume (again with zero energy at reactants), and $Q^{GT}(T,s_*)$ is the generalized transition state partition function with zero energy at $V(s_*)$ and excluding the reaction coordinate. It should be noted that rotational symmetry numbers were removed for all partition functions, as they are included in σ. The symmetry number is computed as[43]

$$\sigma(s) = \frac{n\sigma^R}{\sigma^{GT}(s)} \quad (3)$$

where n is the number of kinetically equivalent transition states, σ^R is the rotational symmetry number for the reactants (or the product of these symmetry numbers if there are two molecular reactants, as in the present case), and $\sigma^{GT}(s)$ corresponds to the

TABLE 1: Classical Potential Energy (ΔV), Adiabatic Potential Energy (ΔV^{AG}), Enthalpy (ΔH^o(298 K)), Entropy (ΔS^o(298 K)), and Free Energy (ΔG^o(298 K)) Values Relative to the Bimolecular Reactants in kcal·mol^{-1}, except for ΔS^o(298 K)(cal·mol^{-1}·K^{-1})[a]

structure	ΔV	ΔV^{AG}	ΔH^o	ΔS^o	ΔG^o
$CF_3CH_2CH_3 + OH$	0.0	0.0	0.0	0.0	0.0
pre_TS1	−2.6	−1.6	−1.6	−15.1	2.9
TS1	4.4	2.2	1.7	−22.1	8.3
post_TS1	−17.2	−17.2	−16.5	−9.1	−13.8
pre_TS2	−2.8	−1.3	−1.5	−19.5	4.3
TS2	4.5	2.5	1.9	−22.5	8.6
post_TS2	−15.6	−15.4	−14.8	−7.7	−12.5
$CF_3CHCH_3 + H_2O$	−13.6	−15.0	−14.3	8.0	−16.7
pre_TSa1	−1.6	−0.4	−0.4	−16.1	4.4
TSa1	4.8	2.6	2.1	−18.1	7.5
post_TSa1	−13.8	−13.7	−13.0	−11.4	−9.6
pre_TSb1	−2.8	−1.3	−1.5	−19.5	4.3
TSb1	3.9	2.0	1.2	−23.1	8.1
post_TSb1	−14.9	−14.2	−14.0	−16.8	−9.0
pre_TSb2					
TSb2	5.8	3.6	3.1	−17.1	8.2
post_TSb2					
$CF_3CH_2CH_2 + H_2O$	−11.7	−13.2	−12.6	5.7	−14.3

[a]The standard state is 1 mol·L^{-1}

usual rotational symmetry number of the generalized transition state at s. In our applications, σ^{GT} is independent of s (because, in practice, it is approximated by the symmetry number at the saddle point), and thus $\sigma(s)$ becomes a constant σ.

Quantum mechanical effects along the reaction coordinate were included by a temperature-dependent transmission coefficient,[40] $\kappa^{MT}(T)$. This coefficient primarily accounts for the multidimensional tunneling. The final CVT/MT rate constant is then given[40] by

$$k^{CVT/MT}(T) = \kappa^{MT}(T)k^{CVT}(T) \quad (4)$$

In the present study, the transmission coefficients, κ^{MT}, were computed using the small curvature tunneling (SCT) approximation.[40] For comparison purposes, further calculations using the zero-curvature tunneling (ZCT)[40] method were carried out.

The MEP in isoinertial mass-scaled Cartesian coordinates was calculated by the Page−McIver algorithm[44] with a gradient stepsize of 0.005 bohr and with the Hessian matrix being recalculated every 10 steps. The partition functions were calculated assuming the rigid rotor-harmonic oscillator approximation. The normal-mode analysis along the reaction path was carried out in rectilinear coordinates. Along the MEPs, some of the lowest generalized normal-mode frequencies became imaginary. The zero-order interpolated variational transition state for frequencies (IVTST0FREQ) algorithm[40] was used to correct them. Then, in all the reaction pathways, the two lowest frequencies were interpolated, except for the TSb2 (see below) pathway, where three imaginary frequencies appeared and had to be interpolated.

All the direct dynamics calculations were carried out using PolyRate 9.4.3[45] and GaussRate 9.4[46] computer programs.

Results and Discussion

Electronic Structure Results. As described below, we have found that both reactions R1 and R2 involve several independent, distinct pathways. In Table 1, the energetics for all the pathways are collected at the stationary points, and Figure 1 shows the geometries of the reactants, the products, and the transition state structures (TSs). For all the pathways, except the one associated with TSb2, pre- and postreactive complexes were located. Going down along the MEP, we have checked that each saddle point is connected with the respective side minima. Their geometries are presented as Supporting Information in Figure S1. In Figure 2 the adiabatic potential energy profiles are shown. Since $CF_3CH_2CH_3$ has C_s symmetry, for reaction R1 (abstraction of a methylenic hydrogen), there is only one type of hydrogen atom; i.e., the two hydrogen atoms of the CH_2 group are equivalent. However, two nonequivalent TSs—TS1 and TS2—were located for reaction R1, both structures having $\sigma = 2$ (that is, $n = 2$, $\sigma^{GT} = 1$, and $\sigma^R = 1$). For reaction R2, which proceeds via H-abstraction from the CH_3 group, the two out-of-plane hydrogen atoms are equivalent. The hydrogen atom in the symmetry plane represents another alternative for hydrogen abstraction. One TS (TSa1) was located for the latter pathway, while two nonequivalent TSs were located for the abstraction of the out-of-plane hydrogen atoms (TSb1 and TSb2). For the three TSs, $\sigma = 2$ (that is, $n = 2$, $\sigma^{GT} = 1$, and $\sigma^R = 1$).

Summarizing, there are five nonequivalent pathways: two for reaction R1, and three for reaction R2 (see Figure 1).

For all the TSs, the following expected patterns are found:

(i) The TS geometries look more similar to reactant geometries than to product structures, as they correspond to a strongly exothermic reaction (Hammond's postulate).

(ii) The C−H bonds that are suffering OH attack are elongated; their bond lengths range from 1.205 Å (TSa1) to 1.213 Å (TS2). The O−H bonds that are being formed are quite longer than the corresponding O−H bond in the water molecule (0.954 Å); their bond lengths range from 1.295 Å (TS1 and TS2) to 1.306 Å (TSa1).

The major structural difference is the presence or absence of hydrogen bonding between the OH hydrogen atom and one of the fluorine atoms in $CF_3CH_2CH_3$. It has been previously demonstrated that hydrogen bonding has a significant effect on the transition states in hydrogen abstraction reactions from fluorinated alkanes.[47] In the present paper, there are three TSs exhibiting hydrogen bonding (TS1, TS2, and TSb1) and two TSs with no hydrogen bonding (TSa1 and TSb2). It is interesting to notice how the hydrogen bonding influences the energetics of the reaction. Considering classical potential energy (V), the lower energetic TSs are those showing hydrogen bonding: TSb1 (3.9 kcal·mol^{-1}), TS1 (4.4 kcal·mol^{-1}), and TS2 (4.5 kcal·mol^{-1}). The inverse order is found when the F···H bond length is considered: TS2 (2.621 Å), TS1 (2.597 Å), and TSb1 (2.381 Å). That is, the stronger the hydrogen bond, the lower the classical barrier.

However, for TSa1, where no hydrogen bond is present, the classical potential energy barrier (4.8 kcal·mol^{-1}) is only slightly higher than the two corresponding to TS1 and TS2. Furthermore, TSb1 is the lowest energy structure out of the three TSs exhibiting hydrogen bonding. Those facts lead us to consider a second factor favoring hydrogen abstraction through CH_3 group versus CH_2 group: charge-transfer.[48,49]

In Figure 3 QTAIM atomic net charges and charge-transfers to the hydroxyl radical for the five TSs are shown. For the two TSs corresponding to reaction R1, the charge-transfers are 0.23 (TS1) and 0.23 (TS2) electrons. For the three TSs of reaction R2, the charge-transfers are 0.25 (TSa1), 0.25 (TSb1), and 0.25 (TSb2) electrons. In the TSs, all the positive charge in excess (on the HFC fragment) is located on the hydrogen that is suffering abstraction. Since the CH_2 group has an electron-withdrawing group attached (CF_3), its C atom contribution to the stabilization of additional positive charge at the H atom is expected to be less important than the corresponding contribu-

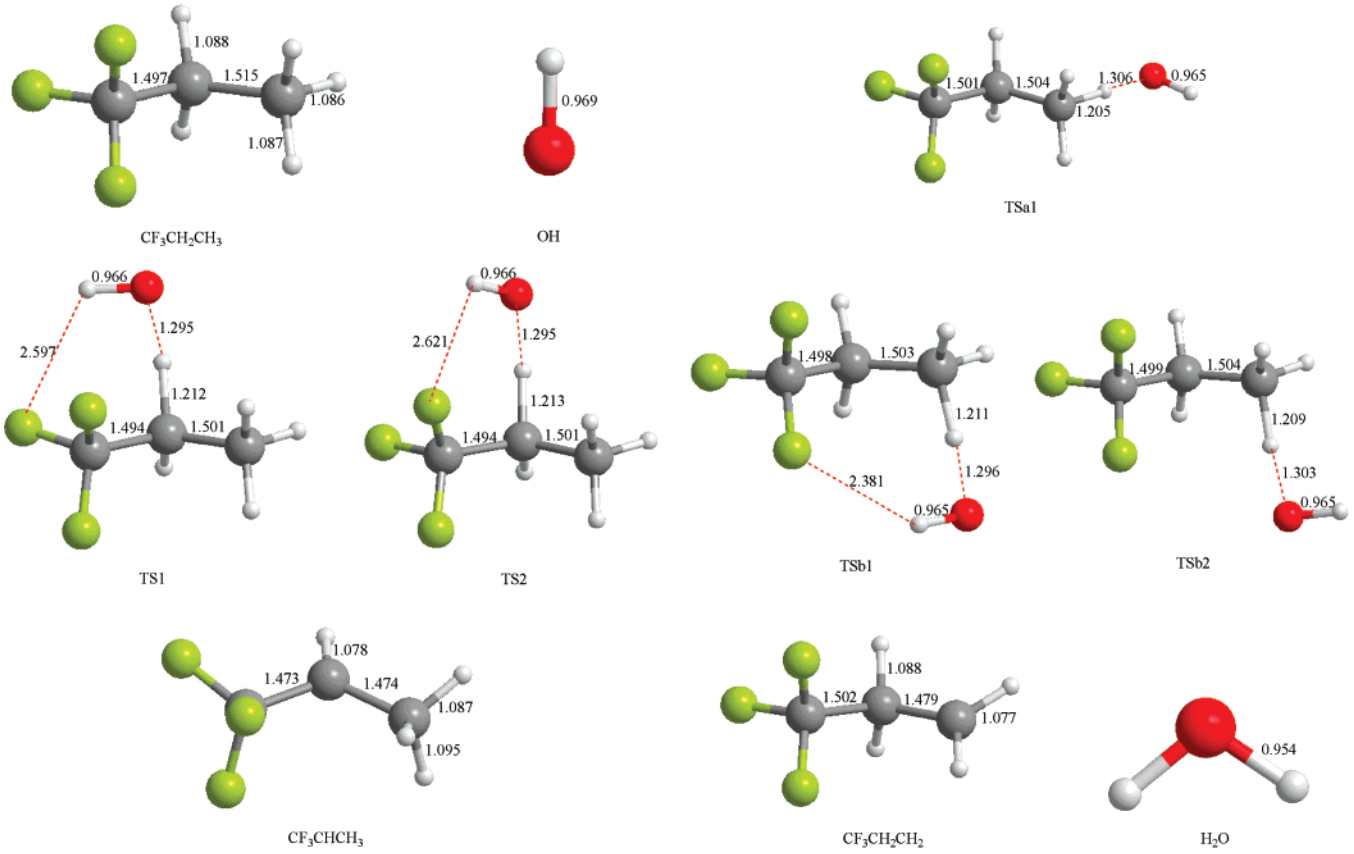

Figure 1. mPW1B95-41.0/6-31+G** geometries for the reactants, products, and TSs. Distances are given in Å.

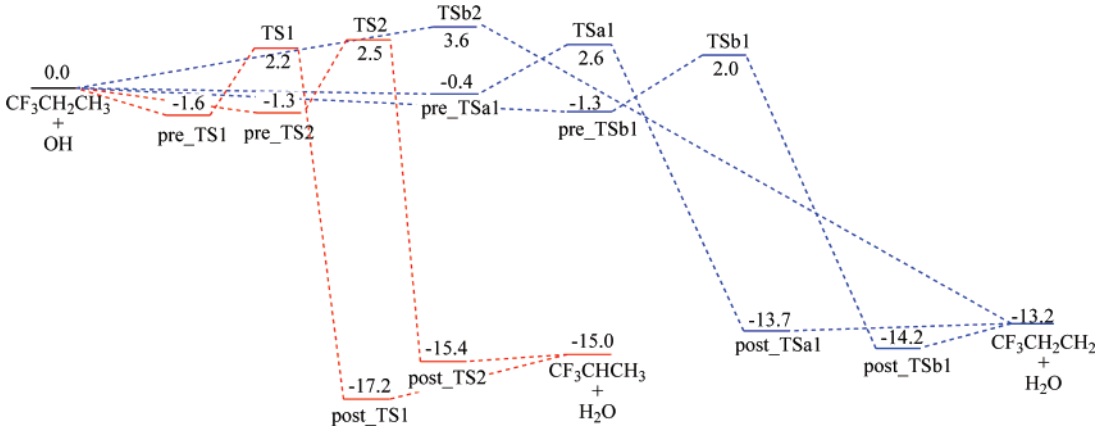

Figure 2. Adiabatic potential energy profiles (kcal/mol) for reactions R1 (red) and R2 (blue).

tion of the C atom in CH_3 group. This explains why charge-transfer for reaction R2 is greater than that for reaction R1.

The classical potential energy barrier of TSb2 is higher than that of TSa1 (5.8 kcal·mol^{-1} vs 4.8 kcal·mol^{-1}). The two factors analyzed above (hydrogen bonding and charge-transfer) cannot be used to explain such a difference. However, a structural consideration allows us to rationalize it. Indeed, for TSa1 and TSb2, the abstraction angles (C···H···O) have values of 178.6° and 172.6°, respectively. Furthermore, TSb2 exhibits a short F···O distance (3.198 Å). Then it seems plausible that electrostatic repulsion between F and O atoms may be the factor making TSb2 higher in energy than TSa1.

Dynamical Results. The overall flux of the $CF_3CH_2CH_3$ + OH reaction is solely determined by the H-abstraction bottlenecks; that is, neither the dynamical bottleneck corresponding to the association processes that lead to the prereactive complexes, nor the dynamical bottlenecks corresponding to the dissociation of the postreactive complexes are kinetically relevant. However, the existence of a complex on the MEP that precedes or follows an H-abstraction TS can be important in the calculation of variational and tunneling effects associated with that H-abstraction bottleneck. The importance of these complexes has already been pointed out.[50] Then, the existence of such complexes has been explicitly taken into account when the corresponding MEPs have been built.

Our results show that, in the five pathways of reactions R1 and R2, important variational effects are present (see Tables 2 and 3). In Table 2, the s value corresponding to the adiabatic potential energy maximum, $s(V^{AG})$, and the $s_*(T)$ values corresponding to the temperature-dependent dynamical bottlenecks are given for each pathway. It can be observed that, in

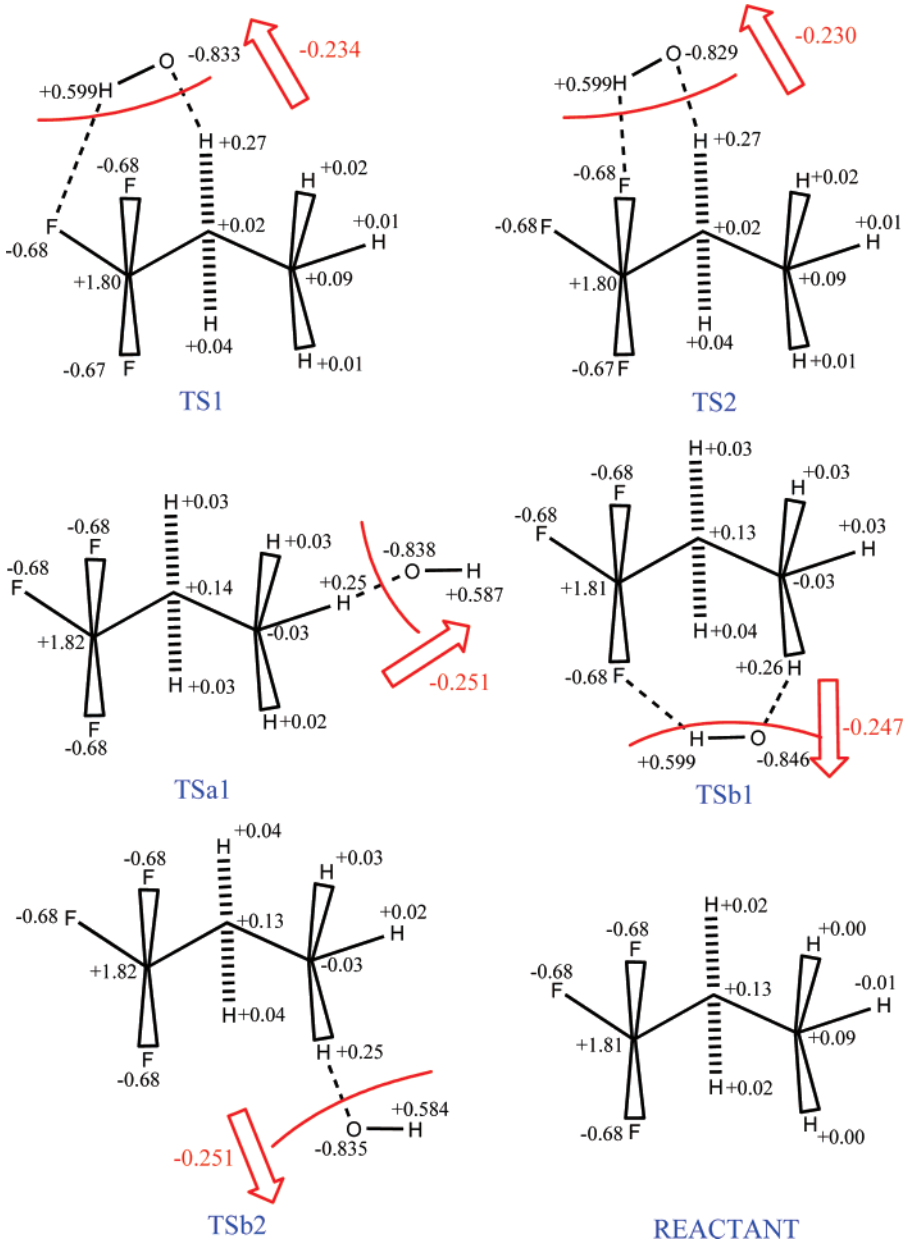

Figure 3. QTAIM atomic net charges and charge-transfer to the hydroxyl radical. Charges are given in a.u.

TABLE 2: Values (in bohr) of $s(V^{AG})$and $s_*(T)$ for the Different Pathways ($s = 0$ at the Corresponding Transition States Structures)

	TS1	TS2	TSa1	TSb1	TSb2
$s(V^{AG})$	−0.35	−0.30	−0.36	−0.26	−0.38
s_*(200 K)	−0.34	−0.28	−0.46	−0.24	−0.30
s_*(238 K)	−0.33	−0.28	−0.47	−0.23	−0.29
s_*(256 K)	−0.33	−0.27	−0.47	−0.23	−0.29
s_*(274 K)	−0.33	−0.27	−0.48	−0.23	−0.28
s_*(297 K)	−0.33	−0.27	−0.49	−0.22	−0.28
s_*(323 K)	−0.33	−0.26	−0.49	−0.22	−0.27
s_*(348 K)	−0.32	−0.26	−0.50	−0.21	−0.26
s_*(373 K)	−0.32	−0.26	−0.50	−0.20	−0.26

all the cases, the dynamical bottleneck is located on the reactants side of the MEP (negative s values).

For the structures with F···H hydrogen bonding (TS1, TS2, TSb1), variational effects are mainly governed by the ZPE. Since this hydrogen bond is present in both the TSs and the prereactive complexes, no dramatic changes in the entropic components along the MEP are expected. Thus, for all the temperatures considered, the CVT activation free-energy maxima are located at no more than 0.06 bohr from $s(V^{AG})$.

Let us now consider the two pathways whose TSs do not involve hydrogen bonding. For TSa1, the dynamical bottleneck is always closer to the reactants than the V_a^G maximum. The higher the temperature, the more separation exists between the two maxima. This fact can be explained by taking into account that the prereactive complex pre_TSa1 (see Figure S1 of Supporting Information) has two weak hydrogen bonds (C−H···O−H), while one of them is broken at the geometry corresponding to the TS TSa1($s = 0$). Then, the prereactive structure is more rigid than the saddle point TSa1, and, consequently, negative entropic contributions are more important for the former, thus shifting the dynamical bottleneck toward reactants. Since entropic effects become more important at higher temperatures, the shifting will be greater as the temperature increases.

For TSb2, the situation is contrary to that of TSa1. For this pathway, no prereactive complex was located, and therefore, as the two reactants approach to form TSb2, the structures

TABLE 3: Experimental and Theoretical Rate Constants (Global Value and Individual Values for Each Pathway in cm^3 molecule^{-1} s^{-1}) vs Temperature[a]

temp	structure	TST	CVT	CVT/ZCT	CVT/SCT	κ^{SCT}	contribution	expt
200 K	TS1	1.49(−15)	1.41(−16)	2.34(−16)	3.04(−16)	2.16	7.4	
	TS2	6.70(−16)	5.07(−17)	1.13(−16)	1.87(−16)	3.69	4.6	
	TSa1	3.38(−15)	2.87(−16)	5.05(−16)	6.61(−16)	2.30	16.0	
	TSb1	2.95(−15)	6.71(−16)	1.52(−15)	2.42(−15)	3.66	60.0	
	TSb2	4.71(−16)	1.28(−16)	2.88(−16)	4.88(−16)	3.80	11.9	
	Global	8.96(−15)	1.28(−15)	2.66(−15)	4.10(−15)			
238 K	TS1	3.94(−15)	5.67(−16)	8.07(−16)	9.66(−16)	1.71	8.4	
	TS2	1.98(−15)	2.20(−16)	3.84(−16)	5.45(−16)	2.48	4.7	
	TSa1	1.09(−14)	1.39(−15)	2.01(−15)	2.43(−15)	1.74	21.1	
	TSb1	6.67(−15)	2.13(−15)	3.76(−15)	5.35(−15)	2.51	46.5	
	TSb2	2.28(−15)	8.97(−16)	1.53(−15)	2.22(−15)	2.48	19.3	
	Global	2.58(−14)	5.21(−15)	8.48(−15)	1.15(−14)			1.96(−14)[b]
256 K	TS1	5.72(−15)	9.62(−16)	1.30(−15)	1.52(−15)	1.58	8.6	
	TS2	2.99(−15)	3.83(−16)	6.19(−16)	8.36(−16)	2.18	4.7	
	TSa1	1.71(−14)	2.53(−15)	3.43(−15)	4.03(−15)	1.60	22.8	
	TSb1	9.12(−15)	3.30(−15)	5.37(−15)	7.31(−15)	2.21	41.3	
	TSb2	4.14(−15)	1.86(−15)	2.90(−15)	4.02(−15)	2.15	22.7	
	Global	3.91(−14)	9.04(−15)	1.36(−14)	1.77(−14)			2.71(−14)[b]
274 K	TS1	7.98(−15)	1.54(−15)	2.00(−15)	2.29(−15)	1.49	8.7	
	TS2	4.32(−15)	6.24(−16)	9.47(−16)	1.23(−15)	1.97	4.7	
	TSa1	2.55(−14)	4.28(−15)	5.51(−15)	6.35(−15)	1.48	24.0	
	TSb1	1.21(−14)	4.87(−15)	7.41(−15)	9.73(−15)	2.00	36.8	
	TSb2	7.00(−15)	3.55(−15)	5.12(−15)	6.82(−15)	1.92	25.8	
	Global	5.69(−14)	1.49(−14)	2.10(−14)	2.64(−14)			3.96(−14)[b]
297 K	TS1	1.17(−14)	2.59(−15)	3.24(−15)	3.63(−15)	1.40	8.6	
	TS2	6.55(−15)	1.08(−15)	1.54(−15)	1.92(−15)	1.77	4.6	
	TSa1	3.99(−14)	7.71(−15)	9.42(−15)	1.06(−14)	1.38	25.2	
	TSb1	1.66(−14)	7.54(−15)	1.07(−14)	1.35(−14)	1.79	32.1	
	TSb2	1.26(−14)	7.27(−15)	9.72(−15)	1.24(−14)	1.71	29.5	
	Global	8.73(−14)	2.62(−14)	3.46(−14)	4.21(−14)			5.55(−14)[b]
298 K	TS1	1.18(−14)	2.65(−15)	3.31(−15)	3.70(−15)	1.40	8.6	
	TS2	6.66(−15)	1.11(−15)	1.57(−15)	1.95(−15)	1.77	4.5	
	TSa1	4.06(−14)	7.89(−15)	9.63(−15)	1.09(−14)	1.38	25.3	
	TSb1	1.68(−14)	7.67(−15)	1.09(−14)	1.37(−14)	1.79	31.9	
	TSb2	1.29(−14)	7.48(−15)	9.97(−15)	1.27(−14)	1.70	29.6	
	Global	8.88(−14)	2.68(−14)	3.54(−14)	4.30(−14)			5.55(−14)[b]
								4.21(−14)[c]
323 K	TS1	1.70(−14)	4.34(−15)	5.24(−15)	5.76(−15)	1.33	8.5	
	TS2	9.89(−15)	1.85(−15)	2.48(−15)	2.99(−15)	1.62	4.4	
	TSa1	6.21(−14)	1.37(−14)	1.60(−14)	1.78(−14)	1.29	26.2	
	TSb1	2.27(−14)	1.16(−14)	1.55(−14)	1.89(−14)	1.63	27.8	
	TSb2	2.25(−14)	1.46(−14)	1.83(−14)	2.25(−14)	1.54	33.2	
	Global	1.34(−13)	4.61(−14)	5.75(−14)	6.79(−14)			8.03(−14)[b]
348 K	TS1	2.35(−14)	6.70(−15)	7.87(−15)	8.53(−15)	1.27	8.3	
	TS2	1.40(−14)	2.91(−15)	3.73(−15)	4.38(−15)	1.51	4.3	
	TSa1	9.04(−14)	2.23(−14)	2.51(−14)	2.74(−14)	1.23	26.7	
	TSb1	2.98(−14)	1.66(−14)	2.11(−14)	2.51(−14)	1.51	24.5	
	TSb2	3.67(−14)	2.62(−14)	3.11(−14)	3.72(−14)	1.42	36.2	
	Global	1.94(−13)	7.47(−14)	8.90(−14)	1.03(−13)			1.07(−13)[b]
373 K	TS1	3.14(−14)	9.85(−15)	1.13(−14)	1.21(−14)	1.23	8.1	
	TS2	1.92(−14)	4.34(−15)	5.37(−15)	6.18(−15)	1.42	4.1	
	TSa1	1.27(−13)	3.42(−14)	3.76(−14)	4.05(−14)	1.19	27.1	
	TSb1	3.81(−14)	2.30(−14)	2.80(−14)	3.26(−14)	1.42	21.8	
	TSb2	5.65(−14)	4.38(−14)	4.98(−14)	5.83(−14)	1.33	38.9	
	Global	2.72(−13)	1.15(−13)	1.32(−13)	1.50(−13)			1.43(−13)[b]

[a] SCT transmission coefficients and the percentage of the contribution from each pathway to the global rate constant are also shown (power of 10 in parentheses). [b] From ref 7. [c] From ref 6.

become more rigid. Then, the dynamical bottleneck is located between the adiabatic maximum and the corresponding classical potential energy maximum (TSb2). As temperature goes up, the dynamical bottleneck moves further toward $s = 0$.

In Table 3, the global and the individual rate constants for each pathway calculated using both the TST and CVT theories are given as a function of temperature. The global rate constant is just the addition of the five individual rate constants corresponding to the five nonequivalent pathways. It can be seen that variational effects reduce the TST rate constants by factors in the range of 0.08−0.27, depending on the particular pathway at 200 K, and by factors from 0.31 to 0.77 at 373 K.

Tunneling effects are not negligible either, although the estimated contributions are much smaller than those expected for this heavy−light−heavy (C···H···O) system. The explanation can be found in Figures S2−S6 of the Supporting Information. Indeed, these figures show that the adiabatic energy curves are rather wide. The shape of those adiabatic profiles reflect the long path that the system has to undertake from the prereactive complexes (or reactants in the TSb2 case) up to the transition-state region, characterized by the heavy atom reorganization and a slow increase of the adiabatic potential energy. The comparison between the ZCT and SCT transmission coefficients shows the influence of reaction path curvature on

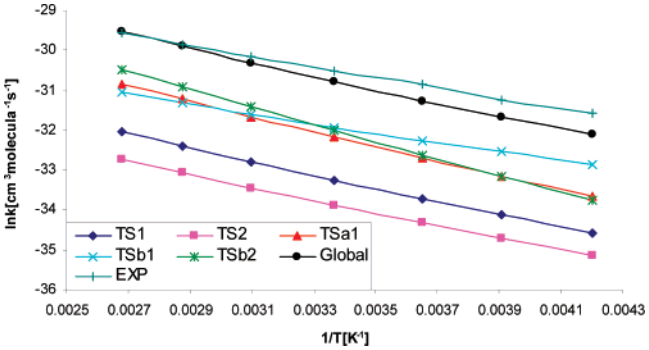

Figure 4. Arrhenius plot for the five pathways and for the global reaction.

the tunneling correction calculation. The validity of this SCT approximation is supported by Albu and Swaminathan, who concluded from their study that H-abstraction reactions from HCFCs by an OH radical are dominated by SCT.[25] So we take the CVT/SCT rate constants as our best theoretical results in this paper.

Table 3 also collects the values for the percentage of the contribution from each pathway to the global rate constant, calculated as

$$\%\ \text{contribution}(i) = \frac{k_i^{\text{CVT/SCT}}}{\sum_j k_j^{\text{CVT/SCT}}} \times 100 \qquad (5)$$

Then, from these contributions, the branching ratios for R1 and R2 can be calculated. For all the temperatures considered, these branching ratios are nearly invariant: 12.0−13.4% for R1 and 86.6−87.9% for R2.

In Figure 4, the Arrhenius plots for the five individual pathways and for the global reaction are shown. It can be observed that the three pathways of reaction R2 are preferred at all temperatures, in comparison with the two R1 pathways. At higher temperatures, the two pathways of R2 denominated as TSa1 and TSb2 are preferred with respect to pathway TSb1 (at higher temperatures, entropic effects dominate over classical barrier heights), whereas the opposite trend occurs at lower temperatures.[49]

The theoretically estimated global rate constant agrees quite well at all temperatures with the experimental values reported by Ravishankara and co-workers.[7] The worst agreement (within 41%) was at 238 K, while the best agreement (within 4%) appears at 348 K. Except for 373 K, the calculated values are slightly lower than the measured ones. As indicated in the Introduction section, at 298 K, two experimental studies for the global rate constant are available. Our theoretical prediction at this temperature is $k^{\text{CVT/SCT}}(298\ \text{K}) = 4.30 \times 10^{-14}$ cm^3 molecule^{-1} s^{-1}, which is in good agreement (within 22.5%) with the value by Ravishankara and co-workers and almost matches (within 2.1%) the experimental measurement by Nelson and co-workers. Taking into account that direct dynamics results using VTST/MT give rate constants that are, on average, within 25−30% of the experimental or the accurate quantum mechanical dynamics rate constants,[51−53] our results are quite good and validate the transferability of the SRP parametrization used for the PES. This transferability of SRP parameters developed for the PM3 method has been already validated by other authors.[24,54]

A linear least-squares fit of the Arrhenius plot for the global rate constant gives an activation energy $E_a = 3.3$ kcal/mol within the range 238−373 K, in good agreement with the value reported by Ravishankara and co-workers (2.6 kcal/mol). Furthermore, also in agreement with the experimental facts, the plot has no significant curvature in the range of temperatures analyzed. Bearing in mind that tunneling contributions are moderate, this is not a surprising result (see Figure 4).

As indicated above, Ravishankara and co-workers used a set of SAR parameters, developed by Tokuhashi and co-workers,[10] to estimate the branching ratios for R1 and R2 with respect to the global rate constant at 298 K. Those equations are based on previous work by Atkinson and co-workers.[9] The value estimated by Ravishankara and co-workers is 4.44×10^{-14} cm^3 molecule^{-1} s^{-1} for the global rate constant, with contributions of 7 and 93% for R1 and R2, respectively. We recalculated those values according to the Tokuhashi procedure, taking into account the number of hydrogen atoms that can be abstracted for each reaction, and we obtained a result of 1.30×10^{-13} cm^3 molecule^{-1} s^{-1} for the global rate constant, with contributions of 4 and 96% for the CH_2 and CH_3 groups, respectively. This rate constant is in poor agreement with the experimental value reported by Ravishankara and co-workers (within 135%), with the one measured by Nelson (within 210%), and with the value calculated in the present work (within 203%).

Ravishankara and co-workers also used the SAR developed by DeMore.[4] With this SAR, a value of 3.01×10^{-14} cm^3 molecule^{-1} s^{-1} for the global rate constant is obtained, and the contributions are predicted to be 55% for the CH_2 group and 45% for the CH_3 group. This rate constant is in moderate agreement (within 45%) with the value by Ravishankara and co-workers, and represents a good agreement with both the experimental value by Nelson and co-workers and the theoretical prediction in the present work (within 28 and 30%, respectively). An improvement for this SAR was reported by DeMore and Wilson.[5] We used those equations, and a value of 4.54×10^{-14} cm^3 molecule^{-1} s^{-1} for the global rate constant is obtained. The branching ratios are 45% for the CH_2 group and 55% for the CH_3 group. The rate constant calculated with this new SAR is in better agreement with the experimental values (within 18 and 8%, with respect to the values reported by Ravishankara and co-workers and by Nelson and co-workers, respectively) and with the computational value (within 6%).

If we compare our calculated rate constants with the two SAR estimates, we can conclude the following:

(i) The SAR by Tokuhashi and co-workers[10] accounts well for the contribution of the CH_2 group, but it overestimates the contribution of the CH_3 group, leading to a rather high global rate constant.

(ii) The two SARs by DeMore and co-workers[4,5] account poorly for the contributions of both groups. However, accidental error compensation results in a good estimate for the global rate constant. In any case, the adiabatic potential energy barriers given in Table 1 show that the branching ratio for R1 and R2 tends roughly to 50% when entropic contributions are not included. As explained above, one of the R2 pathways, the TSb2 one, presents a clearly higher adiabatic potential energy barrier than the other two, TSa1 and TSb1. So, in terms of adiabatic potential energy barriers, both reactions R1 and R2 can be described including just two pathways each, with the four pathways involving quite similar barriers. As a consequence, we can predict that the rate constants of reactions R1 and R2 would become similar at the lowest temperatures.

Conclusions

We have theoretically calculated and analyzed the rate constants for the hydrogen abstraction reaction between OH

radical and $CF_3CH_2CH_3$ from 200 to 373 K using a CVT/SCT direct dynamics approach based on a hybrid meta density functional theory (DFT) parametrized in accordance with an SRP approach. The functional used was adjusted (in a previous work by Albu and Swaminathan) using the CH_3F + OH hydrogen abstraction as a model reaction. The agreement between theory and experiment can be considered quite good, so the transferability of the adjusted DFT to study H-abstraction reactions from more complex HFCs is justified and represents a very promising alternative to the more computationally demanding high-level ab initio methods.

The hydrogen abstraction reaction occurs mainly at the CH_3 group. This reaction contributes over 85% to the global kinetic constant.

We have also compared two kinds of SARs available in the literature with both our computational predictions and the experimental measurements. It has been shown that special care should be exercised when employing SAR methods to make predictions on rate constants and branching ratios.

Acknowledgment. We are grateful for financial support from the Spanish "Ministerio de Educación y Ciencia" and the "Fondo Europeo de Desarrollo Regional" through Projects CTQ2005-07115/BQU and CTQ2004-07405-Co2-02/BQ2, the "Generalitat de Catalunya" (2005SGR00400), and the use of the computational facilities of the CESCA.

Supporting Information Available: Cartesian coordinates for all the structures located on the ab initio potential energy surfaces. Geometries for pre- and postreactive complexes located on the potential energy surfaces. Adiabatic ground-state potential energy curves for the five nonequivalent pathways. Complete references 27 and 45 from the main text. This material is available free of charge via the Internet at http://pubs.acs.org.

References and Notes

(1) *Scientific Assessment of Ozone Depletion 2002*; Global ozone research monitoring project no 47; WMO: Geneva, Switzerland, 2003.

(2) Atkinson, R. In *Air Pollution, the Automobile, and Public Health*; Watson, A. I., Bates, R. R., Kennedy, D., Eds.; National Academic Press: Washington, DC, 1988; pp 99−132.

(3) (a) Jeong, K. M.; Kaufman, F. *J. Phys. Chem.* **1982**, *86*, 1808. (b) Schmoltner, A. M.; Talukdar, R. K.; Warren, R. F.; Mellouki, A.; Goldfard, L.; Gierczak, T.; McKeen, S. A.; Ravishankara, A. R.; *J. Phys. Chem.* **1993**, *97*, 8976. (c) Takular, R.; Mellouki, A.; Gierczak, T.; Burkholder, J. B.; McKeen, S. A.; Ravishankara, A. R. *J. Phys. Chem.* **1991**, *95*, 5815. (d) Wilson, E. W., Jr.; Jacoby, A. M; Kukta, S. J.; Gilbert, L. E.; DeMore, W. B. *J. Phys. Chem. A* **2003**, *107*, 9357.

(4) DeMore, W. B. *J. Phys. Chem.* **1996**, *100*, 5813.

(5) DeMore, W. B.; Wilson, E. W., Jr. *J. Phys. Chem. A* **1999**, *103*, 573.

(6) Nelson, D. D., Jr.; Zahniser, M. S.; Kolb, C. E.; Magid, H. *J. Phys. Chem. A* **1995**, *99*, 16301.

(7) Rajakumar, B.; Portmann, R. W.; Burkholder, J. B.; Ravishankara, A. R. *J. Phys. Chem. A* **2006**, *110*, 6724.

(8) Sabljić, A.; Peijnenburg, W. *Pure Appl. Chem.* **2001**, *73*, 1331.

(9) (a) Atkinson, R. *Int. J. Chem. Kinet.* **1987**, *19*, 799. (b) Kwok, E. S. C.; Atkinson, R. *Atmos. Environ.* **1995**, *29*, 1685.

(10) Tokuhashi, K.; Nagai, H.; Takahashi, A.; Kaise, M.; Kondo, S.; Sekiya, A.; Takahashi, M.; Gotoh, Y.; Suga, A. *J. Phys. Chem. A* **1999**, *103*, 2664.

(11) Urata, S.; Takada, A.; Uchimaru, T.; Chandra, A. K. *Chem. Phys. Lett.* **2003**, *368*, 215.

(12) Percival, C. J.; Marston, G.; Wayne, R. P. *Atmos. Environ.* **1995**, *29*, 305.

(13) Dhanya, S.; Saini, R. D. *Int. J. Chem. Kinet.* **1997**, *29*, 187.

(14) Jeong, K. M.; Kaufman, F. *J. Phys. Chem.* **1982**, *86*, 1816.

(15) (a) Cohen, N.; Benson, S. W. *J. Phys. Chem.* **1987**, *91*, 162. (b) Cohen, N.; Benson, S. W. *J. Phys. Chem.* **1987**, *91*, 171.

(16) Schwartz, M.; Marshall, P.; Berry, R. J.; Ehlers, C. J.; Petersson, G. A. *J. Phys. Chem. A* **1998**, *102*, 10074.

(17) (a) Korchowiec, J.; Kawahara, S.-I.; Matsumura, K.; Uchimara, T.; Surgie, M. *J. Phys. Chem. A* **1999**, *103*, 3548. (b) Korchowiec, J. *J. Phys. Org. Chem.* **2002**, *15*, 524.

(18) Louis, F.; Gonzalez, C. A.; Huie, R. E.; Kurylo, M. J. *J. Phys. Chem. A* **2000**, *104*, 8773.

(19) Fontana, G.; Causà, M.; Gianotti, V.; Marchionni, G. *J. Fluorine Chem.* **2001**, *109*, 113.

(20) Sun, H.; He, H.; Gong, H.; Pan, X.; Li, Z.; Wang, R. *Chem. Phys.* **2006**, *327*, 91.

(21) Zhang, M.; Lin, Z.; Song, C. *J. Chem. Phys.* **2007**, *126*, 034307.

(22) (a) Espinosa-García, J.; Coitiño, E. L.; González-Lafont, À.; Lluch, J. M. *J. Phys. Chem. A* **1998**, *102*, 10715. (b) González-Lafont, À.; Lluch, J. M.; Espinosa-García, J. *J. Phys. Chem. A* **2001**, *105*, 10553. (c) Espinosa-García, J. *J. Phys. Chem. A* **2002**, *106*, 5686.

(23) Lien, P.-Y.; You, R.-M.; Hu, W.-P. *J. Phys. Chem. A* **2001**, *105*, 2391.

(24) Sekušak, S.; Sabljić, A. *J. Phys. Chem. A* **2001**, *105*, 1968.

(25) (a) Albu, T. V.; Swaminathan, S. *J. Phys. Chem. A* **2006**, *110*, 7663. (b) Albu, T. V.; Swaminathan, S. *Theor. Chem. Acc.* **2007**, *117*, 383.

(26) Wang, Y.; Liu, J.-Y.; Yang, L.; Zhao, X.-L.; Ji, Y.-M.; Li, Z.-S. *J. Phys. Chem. A.* **2007**, *111*, 7761.

(27) Frisch, M. J. et al. *Gaussian 03*, revision C.01; Gaussian, Inc.: Wallingford, CT, 2004.

(28) Adamo, C.; Barone, V. *J. Chem. Phys.* **1998**, *108*, 664.

(29) Becke, A. D. *J. Chem. Phys.* **1996**, *104*, 1040.

(30) Perdew, J. P.; Kurth, S. In *A Primer in Density Functional Theory*; Fiolhais, C., Nogueira, F., Marques, M., Eds.; Springer-Verlag: Berlin, 2003.

(31) González-Lafont, À.; Truong, T. N.; Truhlar, D. G. *J. Phys. Chem.* **1991**, *95*, 4618.

(32) Perdew, J. P.; Chervary, J. A.; Vosko, S. H.; Jackson, K. A.; Pederson, M. R.; Singh, D. J.; Fiolhais, C. *Phys. Rev. B* **1992**, *46*, 6671.

(33) Becke, A. D. *Phys. Rev. A.* **1988**, *38*, 3098.

(34) Becke, A. D. *J. Chem. Phys.* **1995**, *98*, 5648.

(35) Lynch, B. J.; Fast, P. L.; Harris, M.; Truhlar, D. G. *J. Phys. Chem. A* **2000**, *104*, 4811.

(36) Zhao, Y.; Lynch, B. J.; Truhlar, D. G. *J. Phys. Chem. A* **2004**, *108*, 2715.

(37) Zhao, Y.; Truhlar, D. G. *J. Phys. Chem. A* **2004**, *108*, 6908.

(38) Bader, R. F. W. *Atoms in Molecules: A Quantum Theory*; Oxford University Press: New York, 1989.

(39) Biegler-König, F. W.; Bader, R. W. F.; Tang, T.-H. *J. Comput. Chem.* **1982**, *3*, 317.

(40) Fernández-Ramos, A.; Miller, J. A.; Klippenstein, S. J.; Truhlar, D. G. *Chem. Rev.* **2006**, *106*, 4518 and references therein.

(41) Truhlar, D. G.; Isaacson, A. D.; Garrett, B. C. In *Theory of Chemical Reactions*; Baer, M., Ed.; CRC Press: Boca Raton, FL, 1985; Vol. 4, p 65 and references therein.

(42) Fukui, K. *Acc. Chem. Res.* **1981**, *14*, 363.

(43) (a) Pechukas, P. *J. Chem. Phys.* **1976**, *64*, 1516. (b) Villà, J.; Corchado, J. C.; González-Lafont, À.; Lluch, J. M.; Truhlar, D. G. *J. Phys. Chem. A* **1999**, *103*, 5061. (c) Masgrau, L.; González-Lafont, À.; Lluch, J. M. *J. Chem. Phys.* **2001**, *114*, 2154.

(44) Page, M.; McIver, J. W., Jr. *J. Chem. Phys.* **1988**, *88*, 922.

(45) Corchado, J. C. et al., *PolyRate*, version 9.4.3; University of Minnesota, Minneapolis, MN, November 2006. http://comp.chem.umn.edu/polyrate.

(46) Corchado, J. C.; Chuang, Y.-Y.; Coitiño, E. L.; Truhlar, D. G. *GaussRate*, version 9.4; University of Minnesota, Minneapolis, MN, June 2006. http://comp.chem.umn.edu/gaussrate.

(47) (a) Martell, J. M.; Boyd, R. J. *J. Phys. Chem.* **1995**, *99*, 13402. (b) Sekušak, S.; Güsten, H.; Sabljić, A. *J. Phys. Chem.* **1996**, *100*, 6212.

(48) Pross, A.; Shaik, S. S. *Acc. Chem. Res.* **1983**, *16*, 363.

(49) Markovic, D.; Varela-Álvarez, A.; Sordo, J. A.; Vogel, P. *J. Am. Chem. Soc.* **2006**, *128*, 7782.

(50) (a) Sekušak, S.; Liedl, K. R.; Rode, B. M.; Sabljić, A. *J. Phys. Chem. A* **1997**, *101*, 4245. (b) Sekušak, S.; Sabljić, A. *Chem. Phys. Lett.* **1997**, *272*, 353. (c) Masgrau, L.; González-Lafont, À.; Lluch, J. M. *J. Comput. Chem.* **1999**, *20*, 1685.

(51) Allison, T. C.; Truhlar, D. G. In *Modern Methods for Multidimensional Dynamics Computations in Chemistry*; Thompson, D. L., Ed.; World Scientific: Singapore, 1998; p 618.

(52) Pu, J.; Corchado, J. C.; Truhlar, D. G. *J. Chem. Phys.* **2001**, *115*, 6266.

(53) Pu, J.; Truhlar, D. G. *J. Chem. Phys.* **2002**, *117*, 1479.

(54) (a) Sekušak, S.; Cory, M. G.; Bartlett, R. J.; Sabljić, A. *J. Phys. Chem. A* **1999**, *103*, 11394. (b) Sekušak, S.; Piecuch, P.; Bartlett, R. J.; Cory, M. G. *J. Phys. Chem. A* **2000**, *104*, 8779.